Cycloolefin Copolymer/Fumed Silica Nanocomposites

Andrea Dorigato,[1] Alessandro Pegoretti,[1] Luca Fambri,[1] Miroslav Slouf,[2] Jan Kolarik[2]

[1]*Department of Materials Engineering and Industrial Technologies, University of Trento, via Mesiano 77, 38123 Trento, Italy*
[2]*Institute of Macromolecular Chemistry, Academy of Sciences of the Czech Republic, 162 06 Prague 6, Czech Republic*

Received 12 March 2010; accepted 19 June 2010
DOI 10.1002/app.32988
Published online 29 September 2010 in Wiley Online Library (wileyonlinelibrary.com).

ABSTRACT: We prepared cycloolefin copolymer (COC)/fumed silica nanocomposites by melt compounding to study the effect of the filler dimensions (filler surface area) on the physical properties, with particular attention to their thermal, mechanical, and optical behaviors. Thermogravimetric analysis revealed a positive contribution of silica nanoparticles to the thermal degradation resistance of COC, as the decomposition temperature of the nanofilled samples increased by 40°C with respect to that of the unfilled matrix. Dynamic mechanical thermal analysis and quasi-static tensile tests of the nanocomposites evidenced a slight stiffening effect, proportional to the nanofiller surface area, without any reduction in the fracture toughness. Creep resistance of the nanocomposites was increased by the addition of silica nanoparticles, especially when high-surface-area nanoparticles were used. The positive effect of the nanoparticles on the viscoelastic and fracture behavior was related to the uniform dispersion of silica aggregates in the matrix. Ultraviolet–visible spectrometry measurements evidenced that the original transparency of neat COC was practically maintained after the addition of silica nanoparticles. © 2010 Wiley Periodicals, Inc. J Appl Polym Sci 119: 3393–3402, 2011

Key words: creep; nanocomposites; polyolefins; silicas

INTRODUCTION

Polymer matrix nanocomposites have increasingly been studied in recent years as novel materials because the incorporation of inorganic nanoparticles into a polymer matrix can significantly improve its physical properties, such as the stiffness,[1–5] stress at break (σ_b),[3,4,6,7] dimensional stability,[8–10] thermal degradation, and chemical resistance,[1,5,6,11] whereas the gas or solvent permeability can be reduced.[11–13] Because significant improvements in the material properties can be achieved at very low filler contents ($\leq$5–10 wt %), the typical drawbacks (embrittlement, loss of transparency, loss of lightness) associated with the addition of traditional inorganic fillers can be avoided.[14,15]

Thermoplastic polymers recently synthesized by means of metallocene-based catalysts have attracted the attention of many researchers and producers.[16–24] Particular interest has been focused on the synthesis and characterization of cycloolefin copolymers (COCs),[14,25–36] which are amorphous thermoplastics obtained by copolymerization of norbornene and ethylene. COCs show remarkable properties, such as stiffness, high chemical resistance, good moisture barrier properties, low moisture absorption, and low density. Because of this unique combination of properties, COCs are suitable for the production of transparent moldings (optical data storage, lenses, and sensors), packaging of drugs, medical and diagnostic devices, food containers, and so on. As the glass-transition temperature (T_g) of COCs can be adjusted by the percentage of norbornene,[37–39] various COC grades suitable for specific applications are available on the market.[40] The polyolefin/COC blends rank among new interesting materials, for example, polypropylene/COC blends[41] with fibrous phase structure and high-density polyethylene/COC blends[42] showing improved dimensional stability.

To our knowledge, only a few articles have been published on the preparation and characterization of COC-based nanocomposites. For example, COC/layered silicate nanocomposites prepared by the intercalation of organically modified layered silicate through a solution mixing process displayed significant improvements in the storage modulus (E') and water permeability with respect to neat COC.[43] COC/silica nanocomposites prepared by solution blending showed certain increases in T_g and the decomposition temperature (T_d) with the silica content and maintained the transparency of the neat matrix.[14,15] Recently, we conducted a detailed analysis of the physical properties of COC/polyhedral oligomeric silsesquioxane nanocomposites and found substantial decreases in the thermal decomposition temperature, the transparency, and the mechanical performance at higher filler contents because of the

Correspondence to: A. Dorigato (andrea.dorigato@ing.unitn.it).

Contract grant sponsor: Grant Agency of the Czech Republic (to J.K.); contract grant number: 106/09/1348.

© 2010 Wiley Periodicals, Inc.

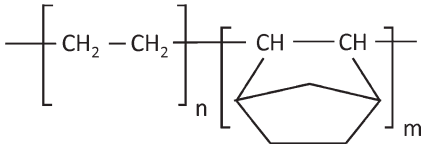

Figure 1 General scheme of the COC repeating units.

presence of a crystalline phase due to polyhedral oligomeric silsesquioxane agglomerates and the formation of a soft interphase at the nanoparticle/polymer boundary.[44] We found no articles in the literature to date dealing with the characterization of COC/fumed silica nanocomposites. It has recently been demonstrated that the addition of small quantities of fumed silica nanoparticles can notably improve the mechanical properties of polyolefin matrices. For instance, fumed silica nanoparticles can substantially enhance the stiffness and fracture toughness of linear low-density polyethylene (LLDPE).[45] Similar results illustrating the role of the surface area of the nanofillers have been reported for poly(methylpentene)/fumed silica nanocomposites.[46]

The objective of this article is to investigate the effect of the incorporation of silica nanoparticles having different specific surface area on the thermal, mechanical, and optical properties of the COC/silica nanocomposites. Particular attention is paid to their thermal degradation resistance, fracture toughness, and creep resistance.

EXPERIMENTAL

Materials and sample preparation

A COC supplied by Ticona (Kelsterbach, Germany), known under the trade name Topas 8007, consisting of 65 wt % ethylene and 35 wt % norbornene (melt flow index at 190°C and 2.16 kg = 1.7 g/10′, density = 1.02 g/cm^3, T_g = 78°C), was used as polymer matrix. Figure 1 reports the chemical structure of the COC used in this study.

Three different kinds of hydrophilic fumed silica nanoparticles, supplied by Degussa (Hanau, Germany), were used as nanofillers: Aerosil 90, Aerosil 200, and Aerosil 380 (A90, A200, and A380, respectively). Their physical properties are summarized in Table I. The density values were measured by a Micromeritics Accupyc 1330 helium pycnometer (Norcross, GA). The specific surface areas were determined with an ASAP 2010 accelerated surface area and porosimetry instrument with the Brunauer–Emett–Teller procedure.[47] From these data, it was possible to calculate the mean diameter (d) of the fumed silica primary nanoparticles according to eq. (1):

$$d = \frac{6000}{\rho \times \mathrm{SSA}} \tag{1}$$

where ρ is the nanofiller density (g/cm^3) and SSA is the specific surface area value (m^2/g). Although the nanofillers presented similar densities, the differences in the reaction conditions during the manufacturing process led to different specific surface area values and primary nanoparticles sizes.

Both polymeric chips and nanofillers were used as received. The silica nanoparticles were melt-mixed with COC in a Thermo Haake Rheomix 600 internal mixer (Karlsruhe, Germany) at 190°C for 15 min with a rotor speed of 90 rpm. Square sheets (width = 200 mm and thickness = 0.7 mm or width = 100 mm and thickness = 4 mm) were obtained by the pressing of the material in proper molds in a Carver laboratory press (Wabash, IN, USA) at 190°C and 0.2 kPa. A filler content of 2 vol % in the composites was chosen on the basis of our previous work on the fracture behavior of LLDPE nanocomposites, which showed maximum ultimate properties at this volume fraction of fumed silica.[48] In this article, the unfilled matrix is denoted as COC, whereas for the nanocomposites, the kind of nanosilica and its content are also reported. For example COC–A200-2 indicates a nanocomposite with 2 vol % A200.

Experimental techniques

Transmission electron microscopy (TEM) observations were performed on thin sections of the investigated nanocomposites ultramicrotomed at −130°C, stained with RuO_4 vapors, and observed at different magnifications with a Vega TS 5130 instrument (Brno, Czech Republic). The mean size of the silica aggregates was evaluated with a public domain, Java-based image processing software (Bethesda, MD), and at least 50 measurements were conducted on the aggregates contained in the TEM images.

TABLE I
Selected Physical Properties of Aerosil-Fumed Silica Nanofillers

Trade name	Nanofiller code	Density (g/cm^3)	Specific surface area (m^2/g)	Estimated primary nanoparticle size (nm)
Aerosil90	A90	2.50 ± 0.01	99.5 ± 0.7	24.1
Aerosil200	A200	2.27 ± 0.02	196.6 ± 1.7	13.4
Aerosil380	A380	2.41 ± 0.02	320.8 ± 3.4	7.8

Thermogravimetric analysis (TGA) was conducted in a Mettler TG50 thermobalance (Schwerzenbach, Switzerland) in the temperature range from 30 to 600°C at a heating rate of 10 K/min. Various atmospheres were considered (nitrogen, air, and oxygen) with a constant flow of 150 mL/min. Dynamic mechanical thermal analysis (DMTA) tests were carried out under a tensile configuration with a MkII Polymer Laboratories analyzer (Loughborough, UK) in the temperature range from 20 to 95°C at a heating rate of 3 K/min on rectangular samples (30 × 5 × 0.7 mm^3). A sinusoidal displacement with a peak-to-peak amplitude of 64 μm and a frequency of 1 Hz was imposed on the samples.

Quasi-static uniaxial tensile tests were performed with an Instron 4502 testing machine (Norwood, MA, USA) equipped with a 1-kN load cell. ISO 527-1BA samples, with a gage length of 30 mm and a width of 5 mm, obtained from the pressed sheets, were tested at a crosshead speed of 1 mm/min. At least five specimens for each sample were tested. The strain was monitored by an Instron 2620-601 clip-on resistance extensometer, with a gage length of 12.5 mm. According to ISO 527 standard, the elastic modulus (E) was determined as a secant value between the strain levels of 0.05 and of 0.25%, that is

$$E = \frac{\sigma_{0.25} - \sigma_{0.05}}{\varepsilon_{0.25} - \varepsilon_{0.05}} \tag{2}$$

where $\sigma_{0.05}$ = stress corresponding to a strain level of 0.05%; $\sigma_{0.25}$ = stress corresponding to a strain level of 0.25%; $\varepsilon_{0.05}$ = strain level 0.05%; $\varepsilon_{0.25}$ = strain level of 0.25%.

Specific tensile energy to break (TEB) values under quasi-static tensile conditions were calculated from the integration of the load–displacement curves with the energy to normalized the samples cross section. Tensile impact tests were conducted on ISO 527-1BA specimens with a CEAST instrumented impact machine (Turin, Italy) with a striker mass of 3.65 kg and an impact speed of 1.25 m/s. Five specimens were tested for each sample.

Three-point flexure tests for the determination of the critical stress intensity factor (K_{IC}) and critical strain energy release rate (G_{IC}) were performed with an Instron 4502 tensile testing machine at a crosshead speed of 10 mm/min. According to ASTM D 5054, single-edge notched samples, 44 mm long, 10 mm wide, and 4 mm thick, were used, with a 5-mm sharp machined notch. At least five specimens for each sample were tested.

Isothermal creep tests were carried out at 30°C with an Instron 4502 testing machine. Rectangular samples, 100 mm long, 5 mm wide, and 0.7 mm thick, with a gage length of 60 mm, were tested at a constant tensile stress (σ_0) equal to 45% σ_b of COC

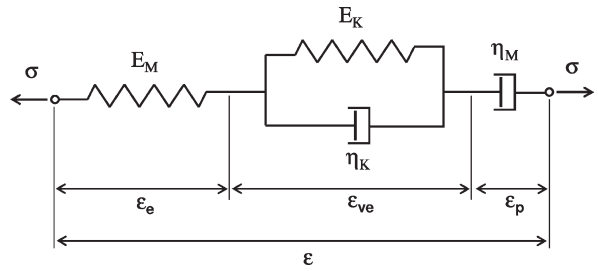

Figure 2 Schematic representation of the Burgers model. σ = applied creep stress; ε_e = elastic component of the creep strain; ε_{ve} = viscoelastic component of the creep strain; ε_p = plastic component of the creep strain; ε = creep strain.

determined from the quasi-static tensile tests. The total duration of a test was 1 h. A tensile creep compliance [$D(t)$] was computed dividing the time-dependent strain [$\varepsilon(t)$] by σ_0. To obtain better comprehension of the creep behavior of the material, the Burgers model was used to interpret the creep data. This model, depicted in Figure 2, consists of a series combination of the Maxwell and Kelvin elements,[49,50] and its constitutive equation under creep condition reads

$$D(t) = \frac{1}{E_M} + \frac{1}{E_K}\left(1 - e^{-\frac{E_K t}{\eta_K}}\right) + \frac{t}{\eta_M} \tag{3}$$

where t is the creep time; E_K and η_K are the elastic and the viscous components in the Kelvin submodel, and E_M and η_M are the analogous parameters for the Maxwell submodel, respectively. The first term of eq. (3) describes the instantaneous elastic compliance (related to the response of the Maxwell submodel), whereas the second term represents the delayed viscoelasticity (accounted by the Kelvin submodel). The third term describes the irreversible viscous flow (if any) in the course of creep.[51]

The transparency of the samples was evaluated with a Jasco V570 spectrometer (Easton, MD). These tests were performed on square samples 0.7 mm thick in a wavelength interval between 200 and 900 nm at a scanning rate of 200 nm/min. The relative transmittance (T%) of neat COC and related nanocomposites was then evaluated over the considered wavelength range, whereas the absorption coefficient of the composites (ε_C) at a certain wavelength (λ) was determined on the basis of Lambert–Beer's law[52]:

$$A = -\log(T) = \varepsilon_C c l \tag{4}$$

where A and T are the absorbance and transmittance, respectively, of the sample at a given wavelength; c is the solute concentration (in our case c = 1); and l is the sample thickness (ca. 0.7 mm). The apparent absorption coefficients of the silica nanoparticles (ε_S^*) were determined as follows:

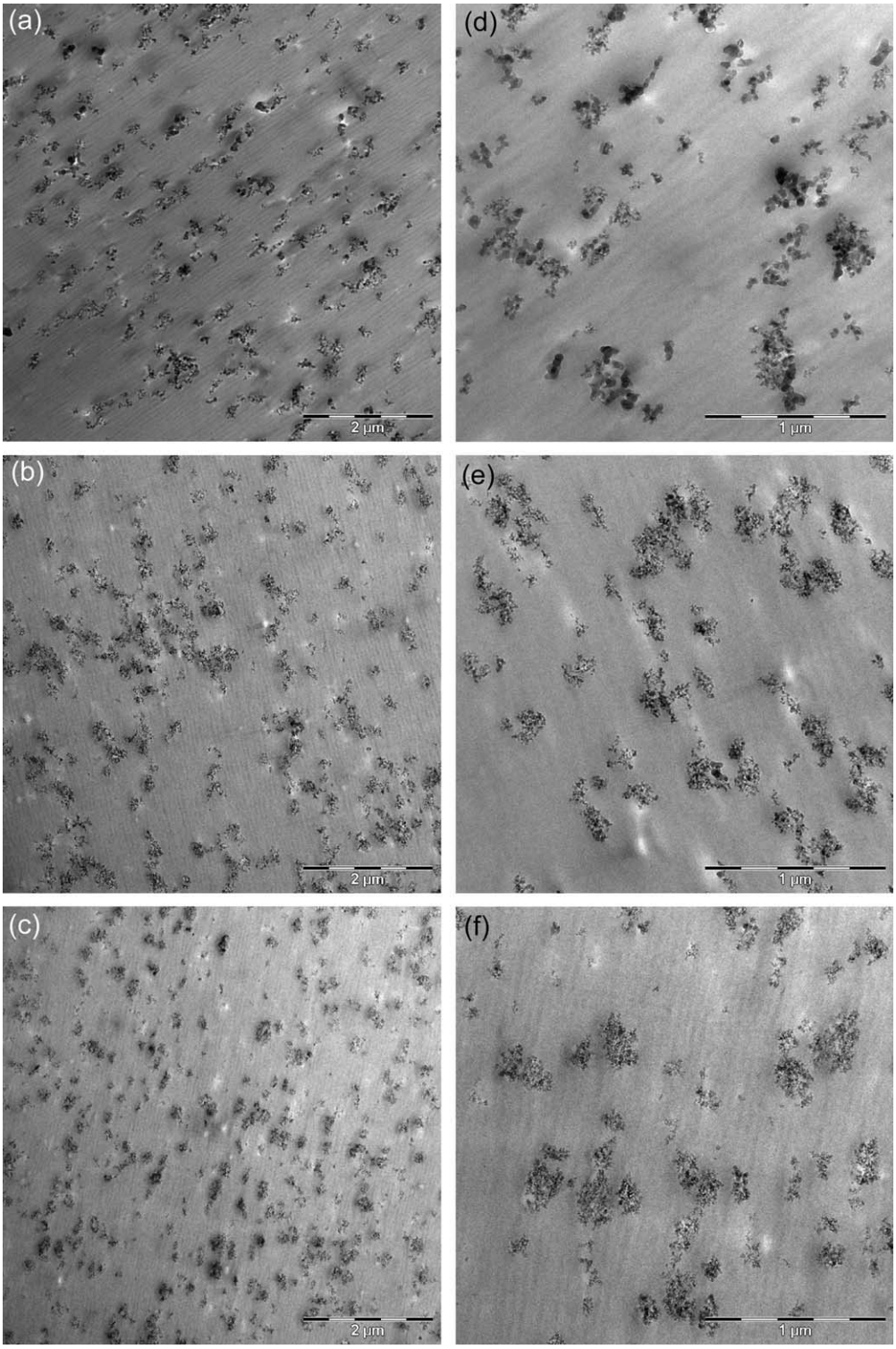

Figure 3 TEM images of the COC/fumed silica nanocomposites at different magnifications: (a–d) COC–A90-2, (b–e) COC–A200-2, and (c–f) COC–A380-2.

$$\varepsilon_S^* = \frac{A_{\text{COMPOSITE}} - A_{\text{COC}}}{cl} \quad (5)$$

where $A_{\text{COMPOSITE}}$ and A_{COC} are the absorbance values of the nanocomposites and neat COC, respectively.

RESULTS AND DISCUSSION

Microstructure characterization

TEM images of nanocomposites are shown in Figure 3; these provided evidence that nanofillers were uniformly dispersed in the matrix and formed

clusters with a mean size lower than 350 nm. However, it was difficult to assess whether the clusters were constituted by aggregation of primary nanoparticles during the manufacturing process or they were formed by physical agglomeration of aggregates. The images at higher magnification showed different sizes of the primary nanoparticles, which were inversely proportional to the surface area of the nanofiller. On the other hand, it was possible to conclude that the mean dimension of the aggregates decreased with increasing surface area of the added silica nanoparticles. In fact, in the case of the COC–A90-2 sample aggregates, a mean diameter of about 300 nm was observed, whereas the COC–A200-2 and COC–A380-2 nanocomposites were characterized by aggregates having a mean size of about 180 and 160 nm, respectively.

To explain this different microstructure, one has to consider that the introduction of fumed silica having different surface areas in polymeric systems generally leads to an enhancement of the shear viscosity values, especially at low shear rates and proportionally to the nanofiller surface area.[53,54] Under these conditions, it is possible that the higher shear forces produced during the melt-compounding process for A380-nanofilled samples could lead to a more effective disruption of silica aggregates and result in a microstructure characterized by aggregates with a lower size.

Thermal and dynamic mechanical characterization

In Figure 4(a), the mass loss as a function of temperature of neat COC and related nanocomposites is reported, whereas in Figure 4(b), the derivative of the mass loss is represented. As shown in Figure 4(b), all of the samples showed an initial decomposition step followed by a second degradation stage at about 400°C, in which the maximum mass loss rate was reached. This thermal behavior was slightly different from that reported in the literature for other COC systems. In fact, Ou and Hsu,[15] in their work on COC silica nanocomposites, showed that both the neat matrix and nanofilled samples decomposed in a single stage; this was attributed to the decomposition of the polymer, whereas pure silica did not present any abrupt decrease in weight. Moreover, the same authors found similar results for the thermogravimetric behavior of COC/silica hybrids prepared by a sol–gel route.[14] To explain this behavior, one has to consider that the chemical structure of the COC copolymer used by the aforementioned authors was constituted by the repetition of monomeric units formed by norbornenic and ethylenic groups. As reported in Figure 1, Topas 8007 is a statistical copolymer in which norbornenic segments are alternated to ethylenic ones. Under these conditions, it was possible that the first mass loss

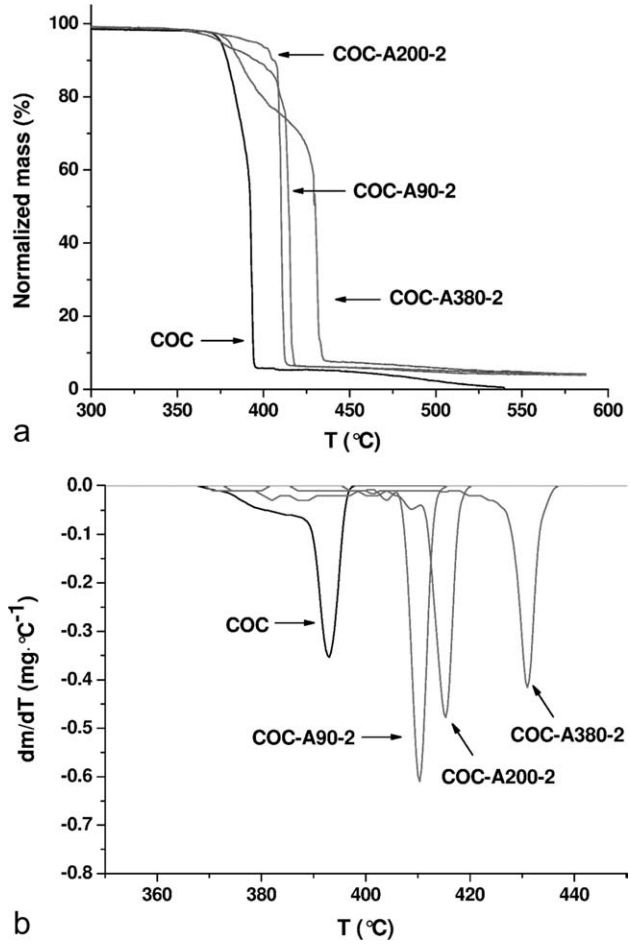

Figure 4 TGA tests on the neat COC and related nanocomposites in oxygen atmosphere: (a) thermogravimetric curves and (b) derivative of the mass loss as a function of the temperature. "m" is the remaining mass during the TGA test.

stage evidenced in the TGA tests was due to the thermal degradation of ethylenic domains possessing a lower thermal stability, whereas the second step was associated with the degradation of norbornenic domains.

In any case, the residual weight fraction of the nanocomposites at 600°C was about 5%, that is, very close to the effective weight percentage of the added silica. From a general point of view, the positive effect of fumed silica on the thermal degradation resistance of the nanocomposites resulted in an increase in the temperatures corresponding to weight losses of 2 and 5% and the maximum degradation rate ($T_{2\%}$, $T_{5\%}$, and T_d, respectively; Table II). Although the improvements observed in nitrogen and air were relatively weak, a more significant enhancement of the thermal stability is achieved in oxygen atmosphere, where T_d is increased by 40°C in the case of COC–A380-2 sample. Even in this case, $T_{2\%}$ and T_d values increase with the surface area of the filler. According to the general theories on the

TABLE II
TGA Data of the Neat COC and Related Nanocomposites

Sample	Nitrogen			Air			Oxygen		
	$T_{2\%}$ (°C)	$T_{5\%}$ (°C)	T_d (°C)	$T_{2\%}$ (°C)	$T_{5\%}$ (°C)	T_d (°C)	$T_{2\%}$ (°C)	$T_{5\%}$ (°C)	T_d (°C)
COC	409	444	474	379	408	449	354	375	390
COC–A90-2	429	446	478	408	427	460	355	375	414
COC–A200-2	430	448	478	408	432	464	363	394	410
COC–A380-2	427	446	476	378	410	458	363	380	430

flame resistance of polymeric nanocomposites,[5,6,55–57] one can hypothesize that silica nanoparticles may act as thermal insulators and limit the diffusion of the oxygen in the materials at high temperatures, making the diffusion path of the oxygen more tortuous and retarding the underlying thermooxidative process. For this reason, a smaller improvement in the thermal stability could be detected for the nanofilled samples under a nitrogen atmosphere, which was consistent with the findings reported in a previous article on the COC/silica nanocomposites.[15] According to TEM images reported in Figure 3, the finer dispersion of silica aggregates observed for COC–A380-2 nanocomposite was responsible for the higher degradation resistance of these samples.

The DMTA measurements reported in Figure 5 indicated that the E' values of nanocomposites [Fig. 5(a)] were slightly higher than that of neat COC over the whole measured temperature range, especially when fumed silicas with higher specific surface areas were incorporated. The stiffening effect provided by the nanoparticles was accompanied by a decrease in the loss tangent (tan δ) peak values [Fig. 5(b)], which were more pronounced for high-surface-area (A380) nanofilled samples. The tan δ peak, corresponding to T_g, indicated a slightly higher (by about 2°C) T_g for the nanocomposites with respect to the neat COC matrix. The literature dealing with the viscoelastic properties of polyolefin-based nanocomposites[58–62] maintains that the increase in the material stiffness and T_g found for nanocomposites can be generally attributed to the reduction of chain mobility due to physical filler/matrix interactions. The higher effectiveness shown by the COC–A380-2 nanocomposite was probably due to a better dispersion of silica clusters in the matrix. Obviously, the presence of a higher number (in a volume unit) of reinforcing elements with smaller dimensions produces a more extensive immobilization of the chains and results in a higher material stiffness.

Tensile properties, fracture, and creep behavior

A slight increase in E brought about by the nanofillers, especially by the high-surface-area silicas, is documented in Figure 6(a) and Table III. The stiffening effect induced by the nanoparticles was accompanied by a slight increase in both the stress and the strain at break, which were proportional to the filler surface area [see Fig. 6(b)].

Furthermore, because the specific TEB values under quasi-static tensile conditions were calculated from the integration of the stress–strain curves, we concluded that the increase in the strength values due to fumed silica introduction was responsible for the enhancement of TEB values detected for the nanofilled samples. In fact, an increase in TEB by

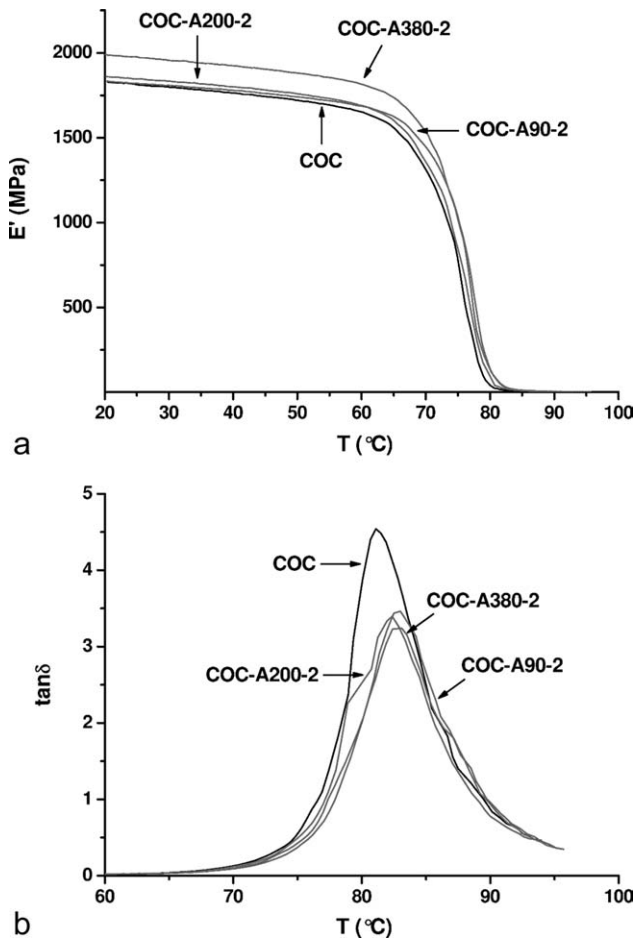

Figure 5 DMTA tests of the neat COC and related nanocomposites (frequency = 1 Hz): (a) E' and (b) tan δ.

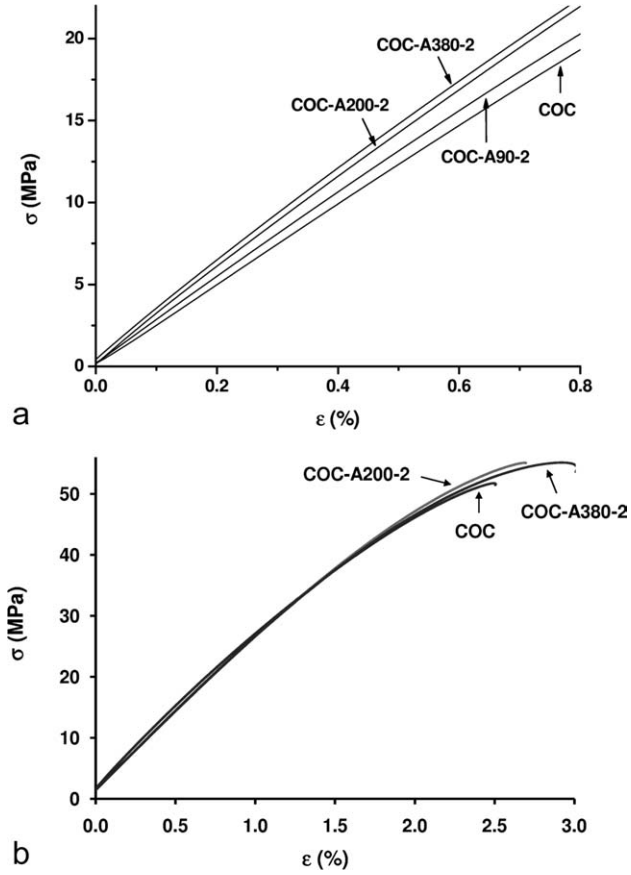

Figure 6 Representative stress–strain curves of the neat COC and related nanocomposites in quasi-static tensile tests (v, crosshead speed = 1 mm/min): (a) evaluation of E and (b) evaluation of the tensile properties at break.

25% with respect to the neat matrix was detected for COC–A380-2 sample. On the other hand, as shown in Figure 7, the specific TEB absorbed under impact conditions was impaired by the introduction of the fumed silica nanoparticles. The different behavior shown by the nanofilled samples under impact conditions could be explained by the fact that the tensile properties at break of thermoplastic materials are very sensitive to strain rate. We interpreted this to mean that under impact conditions, the reinforcing effect provided by the fumed silica nanoparticles was negatively overcome by local stress intensification provided by nanofiller aggregates; this decreased the tensile strain at break.

TABLE III
Quasi-Static Tensile Mechanical Properties of the Neat COC and Related Nanocomposites

Sample	E (GPa)	σ_b (MPa)	ε_b (%)	TEB (mJ/mm^2)
COC	2.57 ± 0.15	51.3 ± 1.4	2.6 ± 0.2	9.9 ± 1.2
COC–A90-2	2.68 ± 0.07	51.3 ± 3.2	2.5 ± 0.2	9.4 ± 1.5
COC–A200-2	2.75 ± 0.20	55.2 ± 0.9	2.5 ± 0.3	10.5 ± 1.6
COC–A380-2	2.72 ± 0.15	54.4 ± 3.1	2.9 ± 0.4	12.4 ± 2.9

ε_b is the tensile strain at break.

Although many articles on polyolefin-based nanocomposites indicate that the stiffening effect induced by inorganic nanoparticles is frequently accompanied by an embrittlement and a reduction in the ultimate tensile properties[8–10]; the general enhancement of the quasi-static ultimate tensile properties induced by fumed silica in our composites was in conformity with the results reported for the LLDPE/fumed silica systems[45] and for polyimides filled by *in situ* generated silica nanoparticles.[63] It seemed likely that the good dispersion of the fumed silica aggregates at the nanoscale level led to relatively lower stress concentration and cracking nucleation phenomena at the interface. For this reason, the COC–A380-2 nanocomposite, characterized by the presence of small aggregates (160 nm), showed the best ultimate properties.

Quantitative assessment of the fracture toughness according to ASTM D 5054 implies the determination of a tentative critical stress intensity factor (K_{IQ}) that can be considered as a K_{IC} value only if the fracture process occurs under the conditions of linear elasticity. The linearity of the load–displacement curves was within the limits imposed by the aforementioned ASTM standard. A limitation on the radius of the plastic zone around the crack tip was also recommended, as expressed by eq. (6), under the plane strain conditions:

$$B, a, (W - a) > 2.5\left(\frac{K_{IQ}}{\sigma_y}\right)^2 \tag{6}$$

where B is the sample thickness, W is the sample width, a is the notch length, and σ_y is the yield stress. As evidenced in the representative force–displacement curves reported in Figure 8(a), both neat COC and nanofilled samples manifested brittle

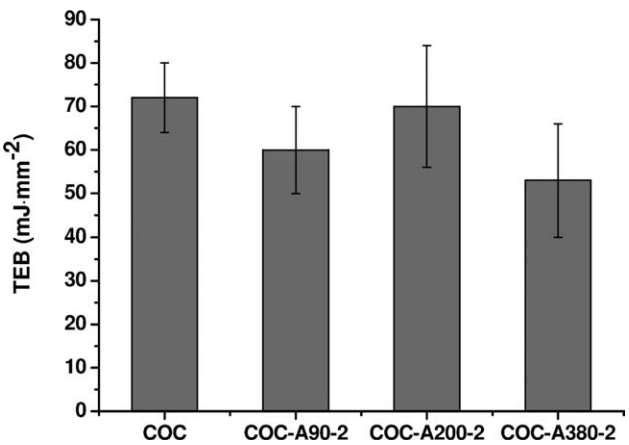

Figure 7 Specific TEB of the neat COC and related nanocomposites under the tensile impact conditions (v = 1.25 m/s).

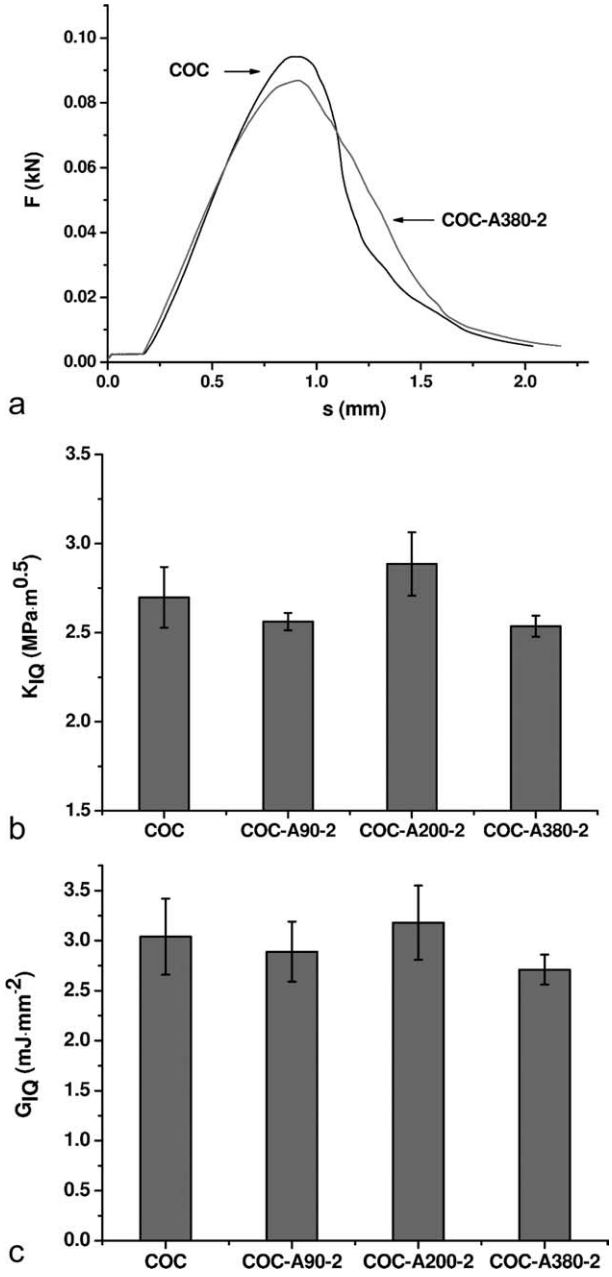

Figure 8 Flexural tests of the single-edge notched samples for the determination of the fracture toughness of the COC and related nanocomposites (v = 10 mm/min): (a) representative force–displacement curves, (b) apparent values of K_{IQ}, and (c) apparent values of G_{IQ}. "F" is the force and "s" is the deflection of the samples registered during the flexural tests.

fracture. For this reason, the maximum stress (σ_{max}) sustained by the samples during quasi-static tensile testing was considered rather than σ_y. Under these conditions, the limitation imposed by eq. (6) was not respected for all of the tested samples. Nevertheless, because plasticization phenomena around the crack tip were very limited, K_{IQ} and G_{IQ} were considered to be reliable estimates of the fracture toughness of the tested materials. As reported in Figure 8(b,c), the

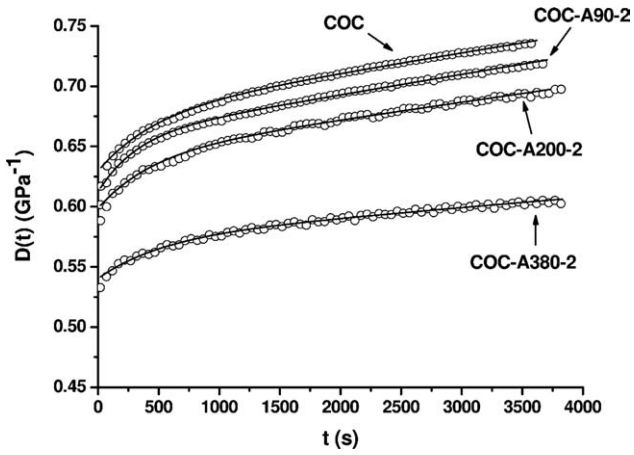

Figure 9 Creep compliance data points for the neat COC and related nanocomposites (temperature = 30°C, σ_0 = 45% σ_{max}). The full lines fit the experimental data by the Burgers model.

K_{IQ} and G_{IQ} values of the nanofilled samples were close to that of the neat matrix, regardless of the nanofiller surface area. We concluded that the silica nanofillers at a volume concentration of 2 vol % did not adversely affect the fracture toughness of the COC matrix, whereas under the quasi-static conditions, a small improvement in the ultimate properties was detected.

In Figure 9, creep compliance curves of COC and related nanocomposites measured at 30°C under a σ_0 equal to 45% σ_b of the unfilled COC matrix are reported. The parameters of the fitting lines corresponding to the Burgers model are given in Table IV. In conformity with dynamic and quasi-static tensile tests, the incorporation of fumed silica led to a significant decrease in the creep compliance, which was proportional to the specific surface area of the nanofiller. Analogous effects of nanosilica on the creep behavior of polymeric nanocomposites observed earlier[4,8,46] were attributed to a restriction in the chain mobility due to polymer/filler physical interactions.[6,10,64,65] As shown, the Burgers model was able to encompass the creep behavior of both COC and related nanocomposites (Fig. 9) over the selected timescale (the R^2 values shown in Table IV

TABLE IV
Parameters of the Burgers Model Fitting the Creep Data of the Neat COC and Related Nanocomposites

Sample	E_K (GPa)	η_K (GPa·s)	E_M (GPa)	η_M (GPa·s)	R^2
COC	14.04	3186	1.67	50972	0.9907
COC–A90-2	12.51	1934	1.75	51012	0.9907
COC–A200-2	14.36	2717	1.77	56332	0.9856
COC–A380-2	21.37	5474	1.92	93014	0.9739

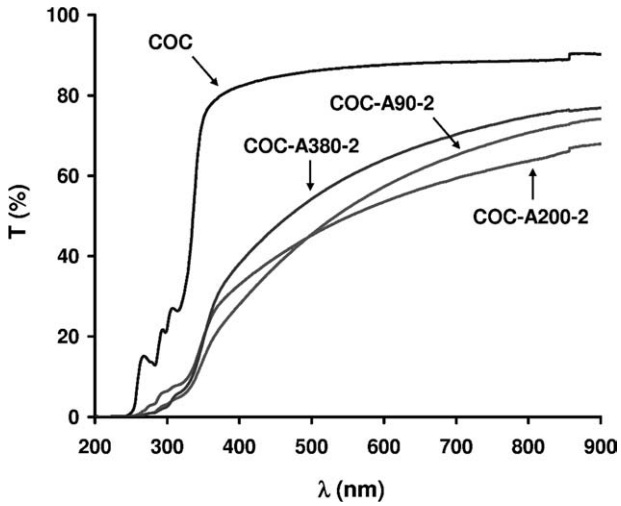

Figure 10 T% as a function of the wavelength of the neat COC and related nanocomposites.

were around 0.98 for all of the tested samples). A slight enhancement in E_M was detected for the nanocomposites with respect to neat COC, which was in accordance with E data from the quasi-static tensile tests. Besides, a consistent increase in the η_M parameter with the surface area of the nanofiller was detected. As the latter parameter controls the long time creep behavior of the materials, we concluded that the positive effect of the incorporated silica nanoparticles was more pronounced at long creep times.

Optical behavior

In Figure 10, the trends of T% as a function of the wavelength found for the COC and related nanocomposites are represented. The ε_C and ε_S^* evaluated by eqs. (5) and (6) are summarized in Table V. The transparency of COC was quite high over the wavelength range in the visible region between 400 and 900 nm, whereas T% values of the nanocomposites decreased (with decreasing wavelength) entering into/approaching the UV region. Even if the differences between the nanofilled samples were not so much pronounced, the COC–A380-2 nanocomposite showed the highest T% values, probably because of the finer size of the filler aggregates. As the T% values of the nanocomposites in the λ interval between 500 and 700 nm were around 50% that of COC, we concluded that the transparency of the COC matrix was not dramatically impaired by the addition of the nanofiller. Also, these optical measurements were conducted on relatively thick (0.7 mm) samples, whereas a good transparency of the COC nanocomposites reported in previous articles[14,15] was evaluated on films 100 μm thick. As shown in Table V, the A380 filled nanocomposite showed the lowest apparent ε_s^* and ε_C values both at $\lambda = 400$ nm and at $\lambda = 700$ nm, which corresponded to the smaller aggregate size and, hence, to the better dispersion of the nanofiller. Obviously, the retention of the optical transparency displayed by the nanofilled samples was important for the production of transparent plastic components with higher thermal and mechanical stability.

CONCLUSIONS

COC-based nanocomposites were prepared through a melt-compounding process with fumed silica nanofillers with different specific surface areas to evaluate their effects on the thermal, mechanical, and optical properties of the resulting materials. TGA demonstrated that nanosilica addition delayed the initial degradation ($T_{2\%}$) of the COC matrix and increased its T_d, especially under an oxygen atmosphere. A slight stiffening effect, manifested by an enhancement of both E' and of E, was detected for the nanofilled samples in DMTA and quasi-static tensile tests, especially when fumed silicas with high surface area values were used. Improved dimensional stability induced by the nanoparticles was confirmed by creep tests, in which a notable decrease in the creep compliance was found for longer creeping times. The fracture toughness was not impaired by the presence of the nanofiller, and a slight increase in the properties at break was detected in the quasi-static tensile tests. The improvement of the mechanical response of the

TABLE V
Absorption Coefficients of the COC (A), Related Nanocomposites (ε_C), and Different Silica Nanoparticles (ε_S^*) [see eqs. (5) and (6)]

Sample	SiO_2 content (wt %)	$\lambda = 400$ nm			$\lambda = 700$ nm		
		A	ε_C (cm^{-1})	ε_S^* (cm^{-1})	A	ε_C (cm^{-1})	ε_S^* (cm^{-1})
COC	0	0.085	1.31	—	0.054	0.83	—
COC–A90-2	4.8	0.553	8.50	360	0.186	2.87	102
COC–A200-2	4.3	0.483	7.43	306	0.226	3.48	132
COC–A380-2	4.6	0.419	6.44	257	0.153	2.36	76

nanocomposites was attributed to the good dispersion of silica nanoscale aggregates, especially when high-surface-area nanosilica was used. The transparency of the original COC was not compromised by the introduction of the nanoparticles because the *T* values in the visible wavelength range only decreased slightly for the nanofilled samples.

The authors thank Chiara Lonardi for her support of their experimental work.

References

1. Mandalia, T.; Bargaya, F. J Phys Chem Solids 2005, 67, 836.
2. Yuan, Q.; Misra, R. D. K. Polymer 2006, 47, 4421.
3. Zhang, J.; Jiang, D. D.; Wilkie, C. A. Thermochim Acta 2005, 430, 107.
4. Zhang, Z.; Yang, J. L.; Friedrich, K. Polymer 2004, 45, 3481.
5. Zhao, C.; Qin, H.; Gong, F.; Feng, M.; Zhang, S.; Yang, M. Polym Degrad Stab 2005, 87, 183.
6. Zhang, M.; Sundararaj, U. Macromol Mater Eng 2006, 291, 697.
7. Zhang, M.; Rong, M. Z.; Zhang, H. B.; Friedrich, K. Polym Eng Sci 2003, 43, 490.
8. Bondioli, F.; Dorigato, A.; Fabbri, P.; Messori, M.; Pegoretti, A. Polym Eng Sci 2008, 48, 448.
9. Pegoretti, A.; Dorigato, A.; Penati, A. Express Polym Lett 2007, 1, 123.
10. Starkova, O.; Yang, J. L.; Zhang, Z. Compos Sci Technol 2007, 67, 2691.
11. Tortora, M.; Gorrasi, M.; Vittoria, G.; Galli, V.; Ritrovati, S.; Chiellini, E. Polymer 2002, 43, 6147.
12. Choi, W. J.; Kim, S. H.; Kim, Y. J.; Kim, S. C. Polymer 2004, 45, 6045.
13. Gorrasi, M.; Tortora, M.; Vittoria, G. J Polym Sci Part B: Polym Phys 2005, 43, 2454.
14. Ou, C. F.; Hsu, M. C. J Appl Polym Sci 2007, 104, 2542.
15. Ou, C. F.; Hsu, M. C. J Polym Res 2007, 14, 373.
16. Arndt, M.; Beulich, I. Macromol Chem Phys 1998, 199, 1221.
17. Donner, M.; Fernandes, M.; Kaminsky, W. Macromol Symp 2006, 236, 193.
18. Kaminsky, W.; Hoff, M.; Derlin, S. Macromol Chem Phys 2007, 208, 1341.
19. Kaminsky, W.; Tran, P. D.; Werner, R. Macromol Symp 2004, 213, 101.
20. Ruchatz, D.; Fink, G. Macromolecules 1998, 31, 4669.
21. Ruchatz, D.; Fink, G. Macromolecules 1998, 31, 4674.
22. Ruchatz, D.; Fink, G. Macromolecules 1998, 31, 4681.
23. Ruchatz, D.; Fink, G. Macromolecules 1998, 31, 4684.
24. Tritto, I.; Boggioni, L.; Jansen, J. C.; Thorshaug, K.; Sacchi, M. C.; Ferro, D. R. Macromolecules 2002, 35, 616.
25. Bergstrom, C.; Ruotoistenmaki, J.; Seppala, J. Polym Test 1997, 16, 43.
26. Chu, P. P. J.; Huang, W. J.; Chang, F. C. Polymer 2001, 42, 2185.
27. Donner, M.; Kiesewetter, J.; Kaminsky, W. J Anal Appl Pyrolysis 2007, 80, 231.
28. Dorkenoo, K. D.; Pfromm, P. H.; Rezac, M. E. J Polym Sci Part B: Polym Phys 1998, 36, 797.
29. Huang, W. J.; Chang, F. C.; Chu, P. P. J. J Polym Sci Part B: Polym Phys 2000, 38, 2554.
30. Huang, W. J.; Chang, F. C.; Chu, P. P. J. Polymer 2000, 41, 6095.
31. Kaminsky, W.; Beulich, I.; Arndt-Rosenau, M. Macromol Symp 2001, 173, 211.
32. Katajisto, J.; Linnolahti, M.; Pakkanen, T. A. Theor Chem Acc 2005, 113, 281.
33. Khanarian, G.; Celanese, H. Opt Eng 2001, 40, 1024.
34. Liu, C.; Yu, J.; Sun, X.; Zhang, J.; He, J. Polym Degrad Stab 2003, 81, 197.
35. Shih, H. H.; Shiao, P. L.; Hsu, H. C. J Appl Polym Sci 2002, 86, 3695.
36. Wendt, R. A.; Mynott, R.; Hauschild, K. Macromol Chem Phys 1999, 200, 1340.
37. Forsyth, J.; Perena, J. M.; Benavente, R. Macromol Chem Phys 2001, 202, 614.
38. Forsyth, J.; Scrivani, T.; Benavente, R. J Appl Polym Sci 2001, 82, 2159.
39. Scrivani, T.; Benavente, R.; Perez, E. Macromol Chem Phys 2001, 202, 2547.
40. McNally, D. In Encyclopedia of Polymer Science and Technology, 3rd ed.; Kroschwitz, J. I.; Mark, H. F. Eds.; Wiley: New York, 2003; Vol. 2, p. 489.
41. Pegoretti, A.; Kolarık, J.; Fambri, L.; Penati, A. Polymer 2003, 44, 3381.
42. Kolarık, J.; Pegoretti, A.; Fambri, L.; Penati, A. Polym Eng Sci 2006, 47, 1363.
43. Wu, T. M.; Wu, C. W. J Polym Sci Part B: Polym Phys 2005, 43, 2745.
44. Dorigato, A.; Pegoretti, A.; Migliaresi, C. J Appl Polym Sci 2009, 114, 2270.
45. Kontou, E.; Niaounakis, M. Polymer 2006, 47, 1267.
46. Dorigato, A.; Pegoretti, A. Polym Int 2010, 59, 719.
47. Brunauer, S.; Emmett, P. H.; Teller, E. J Am Chem Soc 1938, 60, 309.
48. Pegoretti, A.; Dorigato, A.; Penati, A. "Fracture toughness of polyethylene–silica nanocomposites," presented at the 12th International Conference on Fracture (ICF12), Ottawa, Canada, July 12-17th, 2009.
49. McCrum, N. G.; Read, B. E.; Williams, G. Anelastic and Dielectric Effects in Polymeric Solids; Dover: New York, 1984.
50. Riande, E.; Calleja, R. D.; Prolongo, M. G.; Masegosa, R. M.; Salom, C. Polymer Viscoelasticity, Stress and Strain in Practice; Marcel Dekker: New York, 2000.
51. Yang, J. L.; Zhang, Z.; Schlarb, A. K. Polymer 2006, 47, 6745.
52. Silverstein, R. M.; Bassler, G. C.; Morrill, T. C. Spectrometric Identification of Organic Compounds, 4th ed.; Wiley: New York, 1981.
53. Cassagnau, P. Polymer 2008, 49, 2183.
54. Dorigato, A.; Pegoretti, A.; Penati, A. Express Polym Lett 2010, 4, 115.
55. Alexandre, M.; Dubois, P. Mater Sci Eng 2000, 28, 1.
56. Gilman, J. W. Appl Clay Sci 1999, 15, 31.
57. Morgan, A. B. Polym Adv Technol 2006, 17, 206.
58. Gopakumar, T. G.; Lee, J. A.; Kontopoulou, M.; Parent, J. S. Polymer 2002, 43, 5483.
59. Hotta, S.; Paul, D. R. Polymer 2004, 45, 7639.
60. Kato, M.; Okamoto, H.; Hasegawa, N.; Tsukigase, A.; Usuki, A. Polym Eng Sci 2003, 43, 1312.
61. Lee, J. H.; Jung, D.; Hong, C. E.; Rhee, K. Y.; Advani, S. G. Compos Sci Technol 2005, 65, 1996.
62. Wang, K. H.; Choi, M. H.; Koo, C. M.; Xu, M.; Chung, I. J. J Polym Sci Part B: Polym Phys 2002, 40, 1454.
63. Musto, P.; Ragosta, G.; Scarinzi, G.; Mascia, L. Polymer 2004, 45, 4265.
64. Xia, H. S.; Song, M.; Zhang, Z. Y. J Appl Polym Sci 2007, 103, 2992.
65. Zhou, T. H.; Ruan, W. H.; Yang, J. L. Compos Sci Technol 2007, 67, 2297.